Basic cell penetrating peptides induce plasma membrane positive curvature, lipid domain separation and protein redistribution

Ofelia Maniti, Hong-Rong Piao, Jesus Ayala-Sanmartin

Basic cell penetrating peptides induce plasma membrane positive curvature, lipid domain separation and protein redistribution

Ofelia Maniti[1,2,3], Hong-Rong Piao[1,2,3] and Jesus Ayala-Sanmartin[1,2,3]*

[1] CNRS, UMR 7203, Laboratoire de Biomolécules, Groupe N. J. Conté, Paris, France.
[2] École Normale Supérieure, Département de Chimie, 24 rue Lhomond, 75005 Paris France.
[3] Université Pierre et Marie Curie, 4 Place Jussieu, 75252 Paris, France.

* Corresponding author: J. Ayala-Sanmartin, CNRS, UMR 7203, Laboratoire de Biomolécules, Groupe N. J. Conté, 4 Place Jussieu, CP 182, 75252 Paris, France. Tel: 33 1 44 27 38 42. Fax: 33 1 44 27 71 50. E-mail: jesus.ayala-sanmartin@upmc.fr

Abstract

Basic cell penetrating peptides are tools for molecular cellular internalization of non membrane permeable molecules. Their uptake mechanisms involve energy-dependent and energy-independent pathways such as endocytosis, direct translocation or physical endocytosis. These mechanisms are ruled by both, the peptides physicochemical properties and structure and by the membrane lipids characteristics and organisation. Herein we used plasma membrane spheres and membrane models to study the membrane perturbations induced by three arginine-rich cell penetrating peptides. Nona-arginine (R9) and the amphipathic peptide RWRRWWRRW (RW9) induced positive membrane curvature in the form of buds and membrane tubes. Membranous tubes underwent rolling resulting in formation of multilamellar membrane particles at the surface of the plasma membrane spheres. The amphipathic peptides RW9 and RRWRRWWRRWWRRWRR (RW16) provoked lipid and membrane associated protein domain separation as well as changes in membrane fluidity and cholesterol redistribution. These data suggest that membrane domains separation and the formation of multilamellar membranous particles would be involved in arginine-rich cell penetrating peptides internalization.

Keywords: Basic peptides; membrane curvature; membrane domains; membrane rolling; plasma membrane.

Abbreviations: CPP, Cell Penetratin Peptide; GUV, Giant Unilamellar Vesicle; LUV, Large Unilamellar Vesicle; PC, L-α-phosphatidylcholine; PE, L-α-phosphatidylethanolamine; PMS, Plasma Membrane Sphere; PS, L-α-glycerophosphatidyl-L-serine; Py-met-chol, pyrene-labelled methyl-cholesterol; R9, nona-arinine; RW9, RWRRWWRRW; RW16, RRWRRWWRRWWRRWRR.

1. Introduction

The interaction of proteins and peptides with membranes usually provokes a biological response leading to activation of intracellular transport mechanisms, protein transduction and antimicrobial defence. Based on arginine-rich peptide properties, cell penetrating peptides (CPPs) have been developed to carry active molecules into the cytoplasm of eukaryotic cells (Mae and Langel, 2006, Murriel and Dowdy, 2006). It is generally considered that cellular delivery of basic peptides mainly results from two different molecular pathways: direct plasma membrane translocation and internalization by endocytosis with subsequent endosomal release into the cytoplasm (Duchardt et al., 2007, Lundin et al., 2008). Moreover, one peptide can use both pathways depending on its extracellular concentration (Alves et al., 2011, Alves et al., 2008) or on temperature (Jiao et al., 2009). It has also been demonstrated that amphipathic and cationic peptides use different endocytic routes for cellular internalization (Lundin et al., 2008). Recently, it was shown that the formation of membranous particles at the cellular surface is involved in direct arginine-rich peptide penetration into the cytosol (Hirose et al., 2012), and that this phenomenon is favoured by hydrophobic groups on the peptides. Thus, peptide sequence and structure specificities determine the nature of peptide-membrane association and in fine the cellular uptake mechanisms. Therefore, the characterization of peptide-membrane interactions is essential to understand the membrane changes occurring during intracellular traffic and antimicrobial activity as well as the mechanisms of cellular uptake that will help to develop efficient vectors for future therapeutic delivery of molecules.

As *in vivo* phenomena linked to peptide-membrane interactions are complex, work on membrane models allowed to study the biophysical mechanisms and the characterization of peptide structure and affinity for different membranes (Eiriksdottir et al., Maniti et al., 2010, Rydberg et al., 2012, Takechi et al., 2011, Walrant et al., 2012). Several studies showed that basic peptides are able to induce membrane negative curvature resulting in membrane invaginations in the form of vesicles and tubes as well as lipid phase separation (Alves et al., 2008, Lamaziere et al., 2006, Lamaziere et al., 2009, Lamaziere et al., 2010, Lamaziere et al.,

2008, Menger et al., 2003). These peptide-induced membrane deformations would result from changes in membrane asymmetry leading to changes in line tension and bending energy of membrane domains (Lipowsky, 1991, Lipowsky, 1993). Furthermore, insertion of polymers in the membrane increases bilayer asymmetry and produce positive membrane curvature resulting in budding and outward tubulation in Giant Unilamellar Vesicles (GUVs) (Tsafrir et al., 2003). The induction of positive or negative curvature by association of proteins to the membrane has been well established for the so called curvature sensing proteins containing Bar-like domains (Antonny, 2006, Dawson et al., 2006, Saarikangas et al., 2009).

The study of cellular implications of peptide membrane-interactions requires the use of cellular models of the plasma membrane. Giant plasma membrane vesicles (GPMVs) or plasma membrane spheres (PMS) are promising models of biological membranes. These vesicles are void of cellular organelles and nuclear fragments (Scott, 1976) and their spherical morphology allows the observation of membrane deformations. Their molecular composition is representative of the plasma membrane. They contain intrinsic and extrinsic membrane proteins (Baumgart et al., 2007). Their overall lipid composition is typical of the plasma membrane containing phosphatidylcholine (PC), phosphatidylethanolamine (PE), phosphatidylserine (PS) and phosphatidylinositols and, as for the plasma membrane, they are enriched on sphingomyelin (SM) and cholesterol (Fridriksson et al., 1999, Scott, 1976). Not only the global proportion of lipids is conserved but also the proportion of double bonds in acyl chains (Fridriksson et al., 1999). Only two anomalies have been reported: a decrease in phosphatidylinositol-bis-phosphate (Keller et al., 2009) and the loss of PS asymmetry (Baumgart et al., 2007, Keller et al., 2009, Lingwood et al., 2008). However, partial retention of lipid asymmetry has also been reported (Yavin and Zutra, 1979). PMS are able to undergo protein and phospholipid liquid ordered (Lo) and liquid disordered (Ld) phase separation (Baumgart et al., 2007, Keller et al., 2009, Levental et al., 2009, Levental et al., 2011, Lingwood et al., 2008), they are depleted of metabolic energy and membrane cytoskeleton elements are absent (Baumgart et al., 2007, Lingwood et al., 2008). Recently they have been used to study the penetration of several basic cell penetrating peptides (Amand et al., 2011, Maniti et al., 2012, Saalik et al., 2011) and they allowed us to show peptide capacity to induce negative curvature with the consequent formation of plasma membrane invaginations (physical endocytosis) (Maniti et al., 2012).

In the present study we used plasma membrane spheres to characterize the interaction of three different basic peptides with the plasma membrane. Nona-arginine (R9) that penetrate cells efficiently (Futaki et al., 2001, Mitchell et al., 2000, Wender et al., 2000), the amphypathic

peptide RWRRWWRRW (RW9) because it has been shown that the addition of hydrophobic groups and tryptophanes to polyarginines increase cell penetration (Futaki et al., 2001, Hirose et al., 2012, Rydberg et al., 2012), and RRWRRWWRRWWRRWRR (RW16) to study the effect of the length of an amphipathic peptide. We show that the association of small basic peptides with the plasma membrane results in the induction of positive curvature with subsequent vesicle bud formation and membrane tube elongation. Moreover, the membrane tubes underwent rolling and formed membranous particles attached to the plasma membrane surface. These effects were accompanied by changes in membrane fluidity, lipid domain separation and membrane-associated protein (annexin 2) redistribution.

2. Material and Methods

2.1. Materials.

Nona-arginine (R9), RWRRWWRRW (RW9) and RRWRRWWRRWWRRWRR (RW16) where synthesized and purified as described (Lamaziere et al., 2007). Laurdan was from Molecular Probes, di-4-ANNEPDHQ (ANE) was obtained from Dr Leslie M. Loew (Connecticut, USA) and pyrene-labelled cholesterol (Py-met-chol) was a kind gift of Dr. André Lopez (Toulouse, France). Egg yolk L-α-phosphatidylcholine (PC), egg yolk L-α-phosphatidylethanolamine (PE), brain L-α-glycerophosphatidyl-L-serine (PS) and cholesterol were purchased from Sigma-Aldrich.

2.2. Plasma membrane spheres (PMS).

Standard and Annexin 2-GFP transfected MDCK cells were cultured in 75 cm^2 flasks in DMEM in standard conditions (Ayala-Sanmartin et al., 2004). Plasma membrane spheres were obtained by the method described in (Lingwood et al., 2008) adapted in (Maniti et al., 2012). Briefly, PMS induction was performed by overnight incubation of cells with 1 ml of PMS buffer (1.5 mM $CaCl_2$, 1.5 mM $MgCl_2$, 5 mM Hepes, 1 mg ml^{-1} glucose in PBS pH 7.4). After PMS formation, 1 ml of PMS buffer was added, the culture was agitated gently and the supernatant containing the PMS was recovered and centrifuged at 1 000 rpm for 15 min. in a standard Eppendorf centrifuge. The PMS were recovered in 100 µl of PBS and conserved at 4°C for several hours. The experiments presented here were performed with 5 independent PMS preparations.

2.3. Peptide-PMS incubations and treatments.

All preparations for microscopic observation were performed on µ-slide 8 well slides (Ibidi) containing 160 µl of freshly prepared PMS. For di-4-ANEPPDHQ labelling, a stock solution (200 mM) in ethanol was diluted in PBS. Then, 20 µl were added for a final 5 µM concentration. Peptides were added in 10 µl for a final 10 µM concentration. For experiments in hypertonic solution, 20 or 40 µl of sucrose (500 mM) were added to attain a final concentration of 50 and 100 mM sucrose.

2.4. Confocal microscopy.

All confocal images were acquired with a TCS SP2 laser-scanning spectral system (Leica, Wetzlar, Germany) attached to a Leica DMR inverted microscope. Optical sections were recorded with a 63/1.4 or 100/1.4 immersion objectives. We systematically performed 30 confocal slices for each PMS analysed. Considering that most of the PMS were in the range of 15-20 µm, the acquisition of 30 slices allowed the observation of the PMS surface by steps of 500 to 700 nm. Images stacking and 3D-projections were obtained using ImageJ software (NIH). For di-4-ANEPPDHQ imaging, the samples were excited at 488 nm (Ar ion laser) and the fluorescence emission was collected at 570-590 nm for the liquid ordered (Lo) contribution and at 620-640 nm for the liquid disordered (Ld) contribution. Imaging of Annexin 2-GFP was performed by excitation at 488 nm and the emission light was collected at 500-520 nm.

2.5. Quantification of plasma membrane deformations.

The quantification of the different structures observed: tubes, rolled tubes, buds and deformations were performed by direct observation under the microscope. Protrusions were considered as tubes when the length was higher than the diameter. The experiments were performed two to four times. The number of PMS analyzed by direct microscopy was: 1656 for the control PMS, 409 for R9, 1150 for the RW9 and 322 for the RW16 treatments. The number of PMS analyzed by random confocal images were: 88 for the control PMS, 69 for R9, 96 for the RW9 and 69 for the RW16 treatments. The statistical significance was assessed by ANOVA with GraphPad Prism. * $P<0.05$, ** $P<0.01$, *** $P<0.001$.

2.6. Large unilamellar vesicles.

The appropriate amounts of lipids in a mixture of chloroform/methanol, 2/1 (v/v), were subjected to solvent evaporation under nitrogen. Four lipid compositions were used: PC/PS (75/25), PC/PS/cholesterol (50/25/25), PC/PS/PE (25/15/60) and PC/PS/PE/Cholesterol

(17/12/52/19) by weight. Depending on the fluorescence experiments Laurdan was added at 0.1% weight, or Py-met-chol at 3% weight. Lipid films were hydrated with buffer (40 mM Hepes pH 7, 30 mM KCl, 1 mM EGTA) and vortexed extensively to obtain Multilamellar Vesicles (MLVs) at 1 mg/ml. Large Unilamellar Vesicles (LUV) were prepared by extrusion of MLVs through a polycarbonate filter (pore diameter 100 nm) as described (Zibouche et al., 2008).

2.7. Fluorescence spectrometry.

Fluorescence spectra were acquired with a Cary fluorimeter (Varian) as described (Maniti et al., 2010). Temperature was regulated with a Peltier device and controlled by a thermocouple. The excitation and emission band-pass were set at 5 nm. The Laurdan emission spectra were recorded from 400 to 650 nm using 365 nm excitation. The Py-met-chol emission spectra were recorded from 365 to 600 nm using 330 nm excitation. Sequential recorded spectra were: first, 250 µl of buffer (10 mM Hepes pH 7.4) containing 5 µg LUVs, and second the LUVs 10 min. after peptides addition. Spectra were obtained by triplicate and the buffer background was subtracted. The spectra were normalized as 100% for the maximal emission intensity. Peptides were added to a 1:25 peptide:lipid weight ratio (1-2 µM final concentration).

3. Results

3.1.Basic peptides induce membrane budding, outward tubulation and tube rolling.

The interaction with membrane lipids is a crucial step for cell penetrating peptides internalisation. Herein, we analysed peptide-induced membrane deformations using plasma membrane spheres (PMS) (Fig. 1a,b). We studied the efficient cell penetrating peptide R9, a variant with five arginine and 4 tryptophan residues and a longer variant (10 arginine and 6 tryptophane residues). Fig. 1c-f shows that two arginine rich peptides, the fully positive (R9), and the amphipathic (RW9) induced plasma membrane outward budding. The number of buds per PMS and their size were variable ranging from one to more than ten and with a radius from about tenths of µm to several µm (see also supplementary Fig. S1). To characterize accurately the membrane topology of the small buds (external to the PMS), we systematically performed 30 confocal slices for each PMS (see methods). A confocal slice-sequence of a PMS incubated with RW9 showing the conservation of membrane continuity between the PMS and the buds is shown in Movie 1.

Besides the buds, a second type of membrane positive curvature protrusion was observed in the form of long tubes (Fig. 1g-h). Tubes were more frequently observed with the RW9 peptide than with R9. Tube diameters were estimated in the range of ≤0.2 to 1 μm and their length varied from about 5 to more than 100 μm (see also Supplementary Fig. S2). The longer tubes seemed to be associated to PMS containing cellular rests and sometimes it was difficult to discern whether the tube grew from the PMS membrane or the cellular rests. We can assume that cellular rests may act as a reservoir for lipids that supply the growth of very long tubes.

The evolution of tubes and buds is illustrated in Fig. 2. Membrane protrusions (buds and tubes) were observed after 15 min. of peptide incubation. Once the bud or the tube starts to grow at the membrane surface, the process continued for a variable time (from 2 to more than 30 min.) (Fig. 2 and supplementary Figs. S1d, S2c). At the end of the growing process, the protrusions seemed to be stable. In fact we very rarely observed retraction of the buds or tubes for as long as four hours of observation. One example of retraction is shown in Fig. 2d. On the contrary, many of the tubes experimented a rolling process. Fig. 2e and the left part of Fig. 2f show confocal reconstructions of PMS just at the end of the rolling of a tube. Notice the movement of the small circular membranes during rolling. In the right part of Fig. 2f it is shown the PMS at the end of the tube rolling process. Notice that the circular membranes do not move anymore. This phenomenon takes about one second making extremely difficult to capture it by confocal microscopy. One example of such phenomenon occurring during confocal slicing of a PMS is shown in Movie 2.

The frequency of budding and tubulation in more than 3 800 PMS was quantified by microscopy. Not all control PMS were spherically perfect and sometimes bud-like structures were present. Fig. 3 shows that in control and in RW16 treated PMS about 13% of the vesicles presented small protrusions (buds or tubes). When incubated with R9 and RW9 about 21 and 28% of PMS showed protrusions respectively. The statistical analysis revealed that RW9 was the more efficient peptide in provoking protrusions, preferentially tubes (16% of tubes, and 12% of buds), and that R9 was more efficient in provoking bud formation (15% of buds, and 6% of tubes) (Fig. 3). However, the number of tubes was underestimated because as described above, many tubes experimented rolling. Therefore some tubes present in R9 and in RW9 incubated PMS were not counted because we were not sure of the origin of small structures attached to the PMS surface and, for quantification, we considered only

unambiguous buds and extended tubes. Figure 3 show that the number of protrusions observed when PMS were incubated with the longer amphipathic peptide RW16 was smaller compared to RW9 indicating that the amphipathic peptide length is important for the induction of membrane positive curvature.

The formation of membrane protrusions may be influenced by membrane tension. Therefore, because RW9 showed the most efficient induction of protrusions, we studied its budding capacity in PMS at lower membrane tension. To reduce membrane tension, prior to peptide addition, the PMS were incubated in a hypertonic sucrose solution (50 and 100 mM in PBS). As shown in Fig. 4b, RW9 was able to induce membrane budding very efficiently (high number of buds per PMS) indicating that a decrease in membrane tension favours peptide induced budding. At higher sucrose concentrations the PMS changed their morphology spontaneously precluding the analysis of peptide induced budding.

All the precedent experiments were performed with PMS labelled with the fluorescent probe di-4-ANEPPDHQ (ANE). To verify that the peptide induced positive curvature effect was not due to the fluorescent probe insertion in the membrane, we added the RW9 peptide to PMS form cells transfected with the membrane binding protein Annexin 2-GFP (Anx2-GFP). The GFP fluorescence was therefore used as the membrane probe. Fig. 4d shows that RW9 was able to induce plasma membrane budding in the absence of the probe ANE.

3.2. Membrane lipid and protein domain separation induced by basic peptides.

When performing the experiments with Annexin 2-GFP derived PMS we noticed that in several cases the membrane distribution of Anx2-GFP was perturbed by RW9. As shown in Fig. 5a,b, and in Movie 3, RW9 induced a redistribution of Anx2-GFP in Anx2-rich and Anx2-poor membrane domains. Considering that annexin 2 is a protein that binds only acidic phosholipids and that it is present in different membrane domains, we investigated whether the protein separation in domains was accompanied by lipid redistribution. We used the capacity of the ANE probe to sense rigid and fluid domains by changes in fluorescence emission intensities at 570-590 and 620-640 nm respectively (Jin et al., 2006). This probe does not respond to inserted peptides and is thus a good probe for lipid packing (Dinic et al., 2011). In the absence of peptide, small fluid and rigid domains co-exist in the PMS that cannot be easily distinguished and merging of the green (rigid) and red (fluid) fluorescence results in a quite homogeneous yellow colour. With R9 peptide we saw no evident changes in

the ratio of fluorescence intensities at 570-590 and 620-640 nm (membranes homogeneously coloured). With RW9 we observed changes in membrane fluidity in some PMS. In Fig. 2b the PMS core is yellowish by combination of green (570-590 nm ordered lipids contribution) and red (620-640 nm fluid lipids contribution), and the bud is greener indicating a more ordered membrane domain. With RW16 (Fig. 5d-e, supplementary Fig. S3 and in Movies 4 and 5), we observed stronger differences in the 570-590 and 620-640 nm contributions indicating an efficient separation of membrane lipid domains by RW16.

To get more insight into the peptide induced lipid domain separation, we prepared large unilamellar vesicles labelled with Laurdan, a probe able to monitor lipid fluidity by spectral changes. The fluorescence intensities at the maximum emission wavelength in the ordered (440 nm) and disordered (490 nm) phases characterize the spectrum. In LUVs composed of PC alone, the peptides did not induce changes in membrane fluidity (not shown). However, and as shown in Fig. 5f, the addition of peptides in LUVs containing PS induced a relative increase of the ordered (440 nm) contribution. For LUVs containing cholesterol (PC/PS/cholesterol) a relative decrease of the fluid membrane contribution (490 nm) was observed (Fig. S4a). This effect indicates a global decrease of membrane fluidity after peptide binding. We tested other lipid compositions such as PC/PS/PE/cholesterol and the membrane rigidification effect (increase in the ordered contribution) was also observed (Fig. S4b). Notice that in line with the confocal microscopy data, RW16 showed the stronger capacity to reduce membrane fluidity. A second fluorescent probe (Pyrene-labelled cholesterol, Py-met-chol) was used to monitor lipid redistribution. Py-met-chol is able to follow the cholesterol enrichment of a domain by the induction of a fluorescent signal (at 475 nm) corresponding to the packing of the probe as oligomers (excimers) (Le Guyader et al., 2007). We studied the effect of peptides on PC/PS/PE LUVs with and without cholesterol. Fig. 5g and Fig. S4c show that R9 and RW9 induced a small and a moderate reduction of Py-met-chol excimers respectively. The stronger effect was observed with RW16 which decreased the Py-met-chol dimerisation in membranes with and without cholesterol. Overall, these data demonstrate that the basic and, especially the amphipathic peptides, are able to induce lipid and protein redistribution on membranes.

4. Discussion

Direct interaction of molecules with membrane phospholipids can induce diverse membrane deformations with positive or negative curvature as has been shown for Bar and IBar proteins

respectively (Antonny, 2006, Saarikangas et al., 2009). Penetratin and other cell penetrating peptides and toxins were shown to induce negative curvature resulting in membrane invaginations on giant unilamellar vesicles (Lamaziere et al., 2007, Lamaziere et al., 2006, Lamaziere et al., 2008, Romer et al., 2007) and in plasma membrane spheres (Maniti et al., 2012). Herein we studied three peptides; one short basic non structured (R9) and two structured as amphipathic helix, one short (RW9) and one longer (RW16) with different penetration efficacy. The peptide-membrane interaction was studied in LUVs of different composition and in PMS. PMS were used as a plasma membrane model. One important modification of the PMS compared to the plasma membrane of cells is that the PS asymmetry is perturbed inducing a high abnormal PS content at the extracellular surface. This fact would also modify the peptide behaviour compared to the plasma membrane. However, compared to LUVs and GUVs, the PMS, as mentioned in the introduction, contain all the membrane proteins absent in other models and the proportion of lipids and their modifications and molecular diversity are mostly conserved making of them, to our knowledge the closer model of a living cell plasma membrane. The data show that R9 and RW9 are able to induce positive curvature in plasma membrane spheres and that both peptides along with RW16 induce lipid domains reorganization and/or membrane fluidity reduction in PMS and/or LUVs. Each peptide showed particular behaviour indicating that there is a structural specificity of peptide activities and some tendencies were observed and quantified as statistically significant. R9 induced preferentially budding, RW9 induced strong membrane budding and tubulation and RW16 showed the highest lipid domain separation activity. Strong changes in tension and geometry of membranes in the form of tubes rolling were also observed. It is interesting to note that recently it was shown that the direct penetration of polyarginine (R12) into cells is preceded by the formation of membrane particles structured in multilamellar stacks of about 1 μm in diameter on the cellular surface (Hirose et al., 2012), and that the lysine rich peptide S4(13)-PV accumulates also at the cell surface in complex multilamellar structures (Cardoso et al., 2012). Our data suggest that the rolling of tubes observed could be the mechanism leading to multilamellar structures of about 1 μm that would explain the formation of membranous particles observed by others (Hirose et al., 2012) and (Cardoso et al., 2012) and involved in cell penetration. Moreover, the amphipathic peptide RW9 was shown to be more efficient than R9 in tube formation, and as pointed in the Hirose's study (Hirose et al., 2012) membrane particles formation and cell penetration were increased by addition of hydrophobic groups to R12. After formation of multilamellar structures at the cell surface, the molecular mechanism for the final penetration into the cytosol (Hirose et al., 2012) remains unknown.

The authors also suggested that the induction of membrane phase separation upon particle formation may accelerate the peptide penetration into cells. This hypothesis is strongly supported by the membrane domain separation demonstrated in the present study. Overall, positive curvature induction will favour peptide penetration as supported by the fact that R9 and RW9 which provoke stronger curvature are more efficiently internalized than RW16 (Jiao et al., 2009). Moreover, this point is supported by a recent study showing that the membrane positive curvature inducing peptide EPN18 increase the translocation of Alexa488-labeled R8 (Pujals et al., 2013).

What are the molecular mechanisms involved in these peptides-induced membrane changes? The electrostatic interaction of arginines with phospholipids forming guanidine hydrogen bonds seems to be the first step (Rothbard et al., 2004). This interaction would be stable for R9 that remains unstructured upon membrane binding. However, for the peptides RW9 and RW16, the folding as an amphipathic α-helix upon membrane binding (Eiriksdottir et al., Maniti et al., 2010, Rydberg et al., 2012, Takechi et al., 2011, Walrant et al., 2012) would induce an hydrophobic type of interaction involving snorkelling (Mishra and Palgunachari, 1996) of the small RW9 helix, and deeper insertion into the bilayer for the longer peptide RW16.

How positive curvature is induced by these peptides? Membrane budding can be produced by changes in the volume/membrane surface ratio by heating (Dobereiner et al., 1993, Mui et al., 1995). However the differences observed in peptide behaviour cannot be explained by merely heating the samples. The curvature induction mechanism could be based in the increase of membrane bilayer asymmetry. The insertion of molecules in the external leaflet of the bilayer increases its mass and consequently the positive curvature as has been shown for polymers with hydrophobic groups (Tsafrir et al., 2003). A model of the differential peptides action on the membrane is schematized in Fig. 6. R9 will induce a small increase in asymmetry by its interaction with the phospholipid head groups. The induction of positive curvature by R9 does not need the formation of an amphipathic helix. This capacity to create positive curvature without significant membrane insertion is in agreement with a study showing that coating of proteins at the membrane surface without helix insertion into the bilayer can induce membrane tube formation (Stachowiak et al., 2010). RW9 folded as an amphipathic α-helix would snorkel into the external leaflet of the bilayer with a stronger increase in the external leaflet phospholipid spacing inducing higher curvature. This stronger curvature will favour the RW9-mediated formation of tubes with shorter diameter than buds. RW16 is also able to form an amphipathic α-helix and to snorkel, but being longer than RW9, it would be able to

insert into the bilayer perturbing and/or increasing also the internal leaflet mass and therefore inducing a small membrane asymmetry insufficient to provoke significant budding and tubulation. The stronger insertion of RW16 compared to the RW9 peptide is supported by two facts: first, the tryptophan spectral shift observed after membrane binding of RW16 is stronger than that of RW9 (Lamaziere et al., 2007) indicating a more hydrophobic environment for RW16, and second, that, on the contrary to RW9, RW16 is able to permeabilize the membranes inducing the formation of pores in living cells (Lamaziere et al., 2007) and in DOPC and DOPC/DOPG LUVs (Jobin et al.). This membrane permeabilisation would indicate a deeper perturbing interaction of RW16 compared to RW9. The exact mechanism for this behaviour is not known at present but we can speculate that to allow membrane insertion of the amphipathic helix RW16 molecules will associate by their arginines thanks to ionic bridges. This peptide aggregation mediated hypothesis is supported by the fact that RW16 induced membrane permeabilization in LUVs is cooperative (Jobin et al.). Therefore, the differential type of peptide membrane interaction creating different degree of asymmetry would produce weak or strong curvature (buds and/or tubes of different diameter).

From a dynamic point of view, the most remarkable behaviour of membrane tubes was rolling. We suggest that rolling is determined by the capacity of the peptides to aggregate (Lamaziere et al., 2008, Stachowiak et al., 2010). Once the tube is homogeneously covered with the peptide inductor of positive curvature, the tube remains extended. The accumulation of the peptide in one side of the tube will result in a redistribution of the curvature effect. Positive curvature will concentrate on one side and the relaxation of the positive curvature (increase in negative curvature) in the opposite side of the tube will furnish the driving force for rolling (Fig. 6e).

In precedent studies it was shown that short basic peptides were able to induce negative curvature in GUVs (Lamaziere et al., 2008). Herein, R9 and RW9 showed the capacity to induce positive curvature in PMS. Two factors would be responsible for the observed difference between GUVs and PMS. The first is that lipid complexity is stronger in PMS than in the GUVs. We previously show that the peptides were unable to induce negative curvature in Lo phases rich in sphingomyeline and cholesterol in GUVs [17]. The PMS contain higher contents of these lipids and therefore the capacity to induce negative curvature would be also reduced and the positive curvature by bilayer asymmetry (mass increase of the external leaflet) will be allowed. The second factor would be the presence of proteins in the PMS. The absence of proteins in GUVs would favour the movement and clusterization of the peptides

facilitating peptide-lipid reorganization competent for negative curvature. In PMS, the presence of proteins would reduce peptide diffusion and clusterization resulting in preferential membrane asymmetry (by mass increase) and positive curvature effects.

Membrane domain separation was observed by redistribution of the membrane-associated protein annexin 2 as well as by separation of domains with different lipid packing (fluidity). What is the basis of the observed membrane domain separation? First, the different types of interaction (hydrogen bonding for R9, snorkelling for RW9 and bilayer insertion for RW16) with different affinities for phospholipids would result in specific membrane lipids redistribution (Fig. 6). The second factor is that membrane curvature by itself, may induce lipids redistribution as has been shown in GUV membrane tubes obtained by pulling or by photo-oxidation (Roux et al., 2005, Yuan et al., 2008). How peptide-induced lipids redistribution explain the segregation of annexin 2-rich and poor domains in the inner leaflet of the membrane? Molecular modelling suggested that complementary matching of lipids between the inner and the outer leaflet of the membrane take place (Stevens, 2005) and that disturbances of anchored membrane proteins in one leaflet, induce redistribution of proteins in the opposite leaflet (Yue and Zhang, 2012). It has also been demonstrated that cholera toxinB induced lipid separation in the external leaflet provokes redistribution of the cytosolic lipid bound protein Pal-Pal-mCFP (Lingwood et al., 2008). Moreover, it was experimentally shown that changes in one membrane leaflet composition were able to induce domain modification in the other leaflet (Collins and Keller, 2008). Therefore, by coupling between the outer and inner layers, the induced lipids redistribution in one side of the membrane might induce reorganization of lipids domains of different affinity for annexin 2 in the other side of the membrane.

It is known that the membrane geometry and lipids domain separation is a very important factor in cell biology. These processes are involved in most of the membrane related functions especially in vesicular and tubular intracellular transport (Ayala, 1994, Simons and Gerl, 2010, van Meer et al., 2008) and in peptide cell penetration by membrane particle formation at the cell surface (Hirose et al., 2012, Palm-Apergi et al., 2012).

5. Conclusion

In conclusion, basic cell penetrating peptides are able to penetrate cells by different mechanisms: by direct crossing of the plasma membrane, by metabolic endocytosis and by "physical endocytosis" if negative curvature is allowed. In this report we show that basic cell penetrating peptide induce membrane domain reorganization, membrane positive curvature

and the formation of multilamellar membranous particles formed by membrane rolling. These properties should have implications for peptide-mediated intracellular delivery by formation of membranous structures at the cell surface.

Acknowledgments

We thank Philippe Fontanges and Romain Morichon for the confocal facility of the platform Imagerie cellulaire et tissulaire (IFR65 Hôpital Tenon, Paris, France). Dr. André Lopez (Toulouse, France) for the pyrene-labelled cholesterol (Py-met-chol), Antonin Lamazière for peptides and useful comments, and Sandrine Sagan for useful discussions. This study was supported by the Centre National de la Recherche Scientifique (CNRS) and the Université Pierre et Marie Curie.

References

Alves, I. D., Bechara, C., Walrant, A., Zaltsman, Y., Jiao, C. Y. & Sagan, S. (2011). Relationships between membrane binding, affinity and cell internalization efficacy of a cell-penetrating peptide: penetratin as a case study. *PLoS ONE, 6*, e24096.

Alves, I. D., Goasdoue, N., Correia, I., Aubry, S., Galanth, C., Sagan, S., Lavielle, S. & Chassaing, G. (2008). Membrane interaction and perturbation mechanisms induced by two cationic cell penetrating peptides with distinct charge distribution. *Biochim Biophys Acta, 1780*, 948-959.

Amand, H. L., Bostrom, C. L., Lincoln, P., Norden, B. & Esbjorner, E. K. (2011). Binding of cell-penetrating penetratin peptides to plasma membrane vesicles correlates directly with cellular uptake. *Biochim Biophys Acta, 1808*, 1860-1867.

Antonny, B. (2006). Membrane deformation by protein coats. *Curr Opin Cell Biol, 18*, 386-394.

Ayala-Sanmartin, J., Cavusoglu, N., Masliah, J. & Trugnan, G. (2004). Homodimerization of Annexin 2. Role of the N-terminal tail and modulation of membrane aggregation properties. *Annexins, 1*, 19-25.

Ayala, J. (1994). Transport and internal organization of membranes: vesicles, membrane networks and GTP-binding proteins. *J Cell Sci, 107*, 753-763.

Baumgart, T., Hammond, A. T., Sengupta, P., Hess, S. T., Holowka, D. A., Baird, B. A. & Webb, W. W. (2007). Large-scale fluid/fluid phase separation of proteins and lipids in giant plasma membrane vesicles. *Proc Natl Acad Sci U S A, 104*, 3165-3170.

Cardoso, A. M., Trabulo, S., Cardoso, A. L., Lorents, A., Morais, C. M., Gomes, P., Nunes, C., Lucio, M., Reis, S., Padari, K., Pooga, M., Pedroso de Lima, M. C. & Jurado, A. S. (2012). S4(13)-PV cell-penetrating peptide induces physical and morphological changes in membrane-mimetic lipid systems and cell membranes: implications for cell internalization. *Biochim Biophys Acta, 1818*, 877-888.

Collins, M. D. & Keller, S. L. (2008). Tuning lipid mixtures to induce or suppress domain formation across leaflets of unsupported asymmetric bilayers. *Proc Natl Acad Sci U S A, 105*, 124-128.

Dawson, J. C., Legg, J. A. & Machesky, L. M. (2006). Bar domain proteins: a role in tubulation, scission and actin assembly in clathrin-mediated endocytosis. *Trends Cell Biol, 16*, 493-498.

Dinic, J., Biverstahl, H., Maler, L. & Parmryd, I. (2011). Laurdan and di-4-ANEPPDHQ do not respond to membrane-inserted peptides and are good probes for lipid packing. *Biochim Biophys Acta, 1808*, 298-306.

Dobereiner, H. G., Kas, J., Noppl, D., Sprenger, I. & Sackmann, E. (1993). Budding and fission of vesicles. *Biophys J, 65*, 1396-1403.

Duchardt, F., Fotin-Mleczek, M., Schwarz, H., Fischer, R. & Brock, R. (2007). A comprehensive model for the cellular uptake of cationic cell-penetrating peptides. *Traffic, 8*, 848-866.

Eiriksdottir, E., Konate, K., Langel, U., Divita, G. & Deshayes, S. Secondary structure of cell-penetrating peptides controls membrane interaction and insertion. *Biochim Biophys Acta, 1798*, 1119-1128.

Fridriksson, E. K., Shipkova, P. A., Sheets, E. D., Holowka, D., Baird, B. & McLafferty, F. W. (1999). Quantitative analysis of phospholipids in functionally important membrane domains from RBL-2H3 mast cells using tandem high-resolution mass spectrometry. *Biochemistry, 38*, 8056-8063.

Futaki, S., Suzuki, T., Ohashi, W., Yagami, T., Tanaka, S., Ueda, K. & Sugiura, Y. (2001). Arginine-rich peptides. An abundant source of membrane-permeable peptides having potential as carriers for intracellular protein delivery. *J Biol Chem, 276*, 5836-5840.

Hirose, H., Takeuchi, T., Osakada, H., Pujals, S., Katayama, S., Nakase, I., Kobayashi, S., Haraguchi, T. & Futaki, S. (2012). Transient focal membrane deformation induced by arginine-rich peptides leads to their direct penetration into cells. *Mol Ther, 20*, 984-993.

Jiao, C. Y., Delaroche, D., Burlina, F., Alves, I. D., Chassaing, G. & Sagan, S. (2009). Translocation and endocytosis for cell-penetrating peptide internalization. *J Biol Chem, 284*, 33957-33965.

Jin, L., Millard, A. C., Wuskell, J. P., Dong, X., Wu, D., Clark, H. A. & Loew, L. M. (2006). Characterization and application of a new optical probe for membrane lipid domains. *Biophys J, 90*, 2563-2575.

Jobin, M. L., Bonnafous, P., Temsamani, H., Dole, F., Grelard, A., Dufourc, E. J. & Alves, I. D. The enhanced membrane interaction and perturbation of a cell penetrating peptide in the presence of anionic lipids: toward an understanding of its selectivity for cancer cells. *Biochim Biophys Acta, 1828*, 1457-1470.

Keller, H., Lorizate, M. & Schwille, P. (2009). PI(4,5)P2 degradation promotes the formation of cytoskeleton-free model membrane systems. *Chemphyschem, 10*, 2805-2812.

Lamaziere, A., Burlina, F., Wolf, C., Chassaing, G., Trugnan, G. & Ayala-Sanmartin, J. (2007). Non-metabolic membrane tubulation and permeability induced by bioactive peptides. *PLoS ONE, 2*, e201.

Lamaziere, A., Chassaing, G., Trugnan, G. & Ayala-Sanmartin, J. (2006). [Transduction peptides: structural-functional analyses in model membranes]. *J Soc Biol, 200*, 229-233.

Lamaziere, A., Chassaing, G., Trugnan, G. & Ayala-Sanmartin, J. (2009). Tubular structures in heterogeneous membranes induced by the cell penetrating peptide penetratin. *Commun Integr Biol, 2*, 223-224.

Lamaziere, A., Maniti, O., Wolf, C., Lambert, O., Chassaing, G., Trugnan, G. & Ayala-Sanmartin, J. (2010). Lipid domain separation, bilayer thickening and pearling induced by the cell penetrating peptide penetratin. *Biochim Biophys Acta, 1798*, 2223-2230.

Lamaziere, A., Wolf, C., Lambert, O., Chassaing, G., Trugnan, G. & Ayala-Sanmartin, J. (2008). The homeodomain derived peptide Penetratin induces curvature of fluid membrane domains. *PLoS ONE, 3*, e1938.

Le Guyader, L., Le Roux, C., Mazeres, S., Gaspard-Iloughmane, H., Gornitzka, H., Millot, C., Mingotaud, C. & Lopez, A. (2007). Changes of the membrane lipid organization characterized by means of a new cholesterol-pyrene probe. *Biophys J, 93*, 4462-4473.

Levental, I., Byfield, F. J., Chowdhury, P., Gai, F., Baumgart, T. & Janmey, P. A. (2009). Cholesterol-dependent phase separation in cell-derived giant plasma-membrane vesicles. *Biochem J, 424*, 163-167.

Levental, I., Grzybek, M. & Simons, K. (2011). Raft domains of variable properties and compositions in plasma membrane vesicles. *Proc Natl Acad Sci U S A, 108*, 11411-11416.

Lingwood, D., Ries, J., Schwille, P. & Simons, K. (2008). Plasma membranes are poised for activation of raft phase coalescence at physiological temperature. *Proc Natl Acad Sci U S A, 105*, 10005-10010.

Lipowsky, R. (1991). The conformation of membranes. *Nature, 349*, 475-481.

Lipowsky, R. (1993). Domain-induced budding of fluid membranes. *Biophys J, 64*, 1133-1138.

Lundin, P., Johansson, H., Guterstam, P., Holm, T., Hansen, M., Langel, U. & S, E. L. A. (2008). Distinct uptake routes of cell-penetrating peptide conjugates. *Bioconjug Chem, 19*, 2535-2542.

Mae, M. & Langel, U. (2006). Cell-penetrating peptides as vectors for peptide, protein and oligonucleotide delivery. *Curr Opin Pharmacol, 6*, 509-514.

Maniti, O., Alves, I., Trugnan, G. & Ayala-Sanmartin, J. (2010). Distinct behaviour of the homeodomain derived cell penetrating peptide penetratin in interaction with different phospholipids. *PLoS ONE, 5*, e15819.

Maniti, O., Blanchard, E., Trugnan, G., Lamaziere, A. & Ayala-Sanmartin, J. (2012). Metabolic energy-independent mechanism of internalization for the cell penetrating peptide penetratin. *Int J Biochem Cell Biol, 44*, 869-875.
Menger, F. M., Seredyuk, V. A., Kitaeva, M. V., Yaroslavov, A. A. & Melik-Nubarov, N. S. (2003). Migration of poly-L-lysine through a lipid bilayer. *J Am Chem Soc, 125*, 2846-2847.
Mishra, V. K. & Palgunachari, M. N. (1996). Interaction of model class A1, class A2, and class Y amphipathic helical peptides with membranes. *Biochemistry, 35*, 11210-11220.
Mitchell, D. J., Kim, D. T., Steinman, L., Fathman, C. G. & Rothbard, J. B. (2000). Polyarginine enters cells more efficiently than other polycationic homopolymers. *J Pept Res, 56*, 318-325.
Mui, B. L., Dobereiner, H. G., Madden, T. D. & Cullis, P. R. (1995). Influence of transbilayer area asymmetry on the morphology of large unilamellar vesicles. *Biophys J, 69*, 930-941.
Murriel, C. L. & Dowdy, S. F. (2006). Influence of protein transduction domains on intracellular delivery of macromolecules. *Expert Opin Drug Deliv, 3*, 739-746.
Palm-Apergi, C., Lonn, P. & Dowdy, S. F. (2012). Do cell-penetrating peptides actually "penetrate" cellular membranes? *Mol Ther, 20*, 695-697.
Pujals, S., Miyamae, H., Afonin, S., Murayama, T., Hirose, H., Nakase, I., Taniuchi, K., Umeda, M., Sakamoto, K., Ulrich, A. S. & Futaki, S. (2013). Curvature engineering: positive membrane curvature induced by epsin N-terminal Peptide boosts internalization of octaarginine. *ACS Chem Biol, 8*, 1894-1899.
Romer, W., Berland, L., Chambon, V., Gaus, K., Windschiegl, B., Tenza, D., Aly, M. R., Fraisier, V., Florent, J. C., Perrais, D., Lamaze, C., Raposo, G., Steinem, C., Sens, P., Bassereau, P. & Johannes, L. (2007). Shiga toxin induces tubular membrane invaginations for its uptake into cells. *Nature, 450*, 670-675.
Rothbard, J. B., Jessop, T. C., Lewis, R. S., Murray, B. A. & Wender, P. A. (2004). Role of membrane potential and hydrogen bonding in the mechanism of translocation of guanidinium-rich peptides into cells. *J Am Chem Soc, 126*, 9506-9507.
Roux, A., Cuvelier, D., Nassoy, P., Prost, J., Bassereau, P. & Goud, B. (2005). Role of curvature and phase transition in lipid sorting and fission of membrane tubules. *Embo J, 24*, 1537-1545.
Rydberg, H. A., Matson, M., Amand, H. L., Esbjorner, E. K. & Norden, B. (2012). Effects of tryptophan content and backbone spacing on the uptake efficiency of cell-penetrating peptides. *Biochemistry, 51*, 5531-5539.
Saalik, P., Niinep, A., Pae, J., Hansen, M., Lubenets, D., Langel, U. & Pooga, M. (2011). Penetration without cells: membrane translocation of cell-penetrating peptides in the model giant plasma membrane vesicles. *J Control Release, 153*, 117-125.
Saarikangas, J., Zhao, H., Pykalainen, A., Laurinmaki, P., Mattila, P. K., Kinnunen, P. K., Butcher, S. J. & Lappalainen, P. (2009). Molecular mechanisms of membrane deformation by I-BAR domain proteins. *Curr Biol, 19*, 95-107.
Scott, R. E. (1976). Plasma membrane vesiculation: a new technique for isolation of plasma membranes. *Science, 194*, 743-745.
Simons, K. & Gerl, M. J. (2010). Revitalizing membrane rafts: new tools and insights. *Nat Rev Mol Cell Biol, 11*, 688-699.
Stachowiak, J. C., Hayden, C. C. & Sasaki, D. Y. (2010). Steric confinement of proteins on lipid membranes can drive curvature and tubulation. *Proc Natl Acad Sci U S A, 107*, 7781-7786.
Stevens, M. J. (2005). Complementary matching in domain formation within lipid bilayers. *J Am Chem Soc, 127*, 15330-15331.
Takechi, Y., Yoshii, H., Tanaka, M., Kawakami, T., Aimoto, S. & Saito, H. (2011). Physicochemical mechanism for the enhanced ability of lipid membrane penetration of polyarginine. *Langmuir, 27*, 7099-7107.
Tsafrir, I., Caspi, Y., Guedeau-Boudeville, M. A., Arzi, T. & Stavans, J. (2003). Budding and tubulation in highly oblate vesicles by anchored amphiphilic molecules. *Phys Rev Lett, 91*, 138102.
van Meer, G., Voelker, D. R. & Feigenson, G. W. (2008). Membrane lipids: where they are and how they behave. *Nat Rev Mol Cell Biol, 9*, 112-124.

Walrant, A., Vogel, A., Correia, I., Lequin, O., Olausson, B. E., Desbat, B., Sagan, S. & Alves, I. D. (2012). Membrane interactions of two arginine-rich peptides with different cell internalization capacities. *Biochim Biophys Acta, 1818*, 1755-1763.

Wender, P. A., Mitchell, D. J., Pattabiraman, K., Pelkey, E. T., Steinman, L. & Rothbard, J. B. (2000). The design, synthesis, and evaluation of molecules that enable or enhance cellular uptake: peptoid molecular transporters. *Proc Natl Acad Sci U S A, 97*, 13003-13008.

Yavin, E. & Zutra, A. (1979). Translocation and turnover of phospholipid analogs in plasma membrane-derived vesicles from cell cultures. *Biochim Biophys Acta, 553*, 424-437.

Yuan, J., Hira, S. M., Strouse, G. F. & Hirst, L. S. (2008). Lipid bilayer discs and banded tubules: photoinduced lipid sorting in ternary mixtures. *J Am Chem Soc, 130*, 2067-2072.

Yue, T. & Zhang, X. (2012). Signal transduction across cellular membranes can be mediated by coupling of the clustering of anchored proteins in both leaflets. *Phys Rev E Stat Nonlin Soft Matter Phys, 85*, 011917.

Zibouche, M., Vincent, M., Illien, F., Gallay, J. & Ayala-Sanmartin, J. (2008). The N-terminal domain of annexin 2 serves as a secondary binding site during membrane bridging. *J Biol Chem, 283*, 22121-22127.

Figures legends

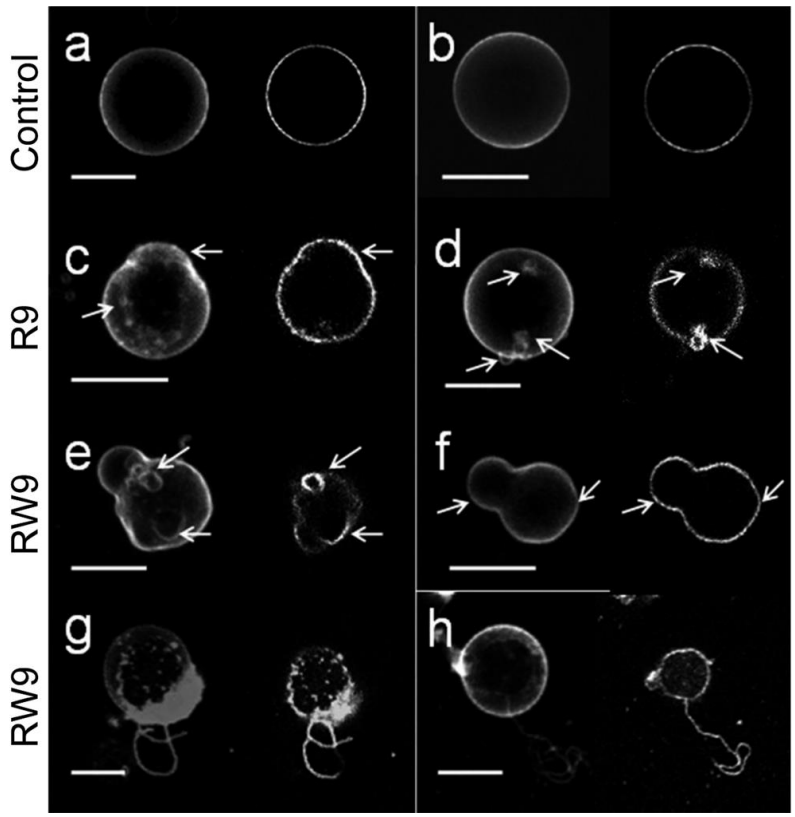

Fig. 1 Basic peptides induce membrane protrusions on PMS. Confocal images of PMS labelled with the fluorescent probe di-4-ANEPPDHQ. Peptide-free PMS at 15 (**a**) and 180 min. (**b**) after di-4-ANEPPDHQ addition. PMS incubated with R9 (**c,d**), and RW9 (**e,f**). At the left of the panels are the projections of 30 confocal slices, and at right a selected slice. Notice that the apparent internal vesicles are buds from the plasma membrane. Some buds are pointed by arrows (see also movie 1). Membrane tubes from PMS after incubation with RW9 (**g**,**h**). Notice the different length and diameter of the membrane protrusions. Scale bars 10 μm

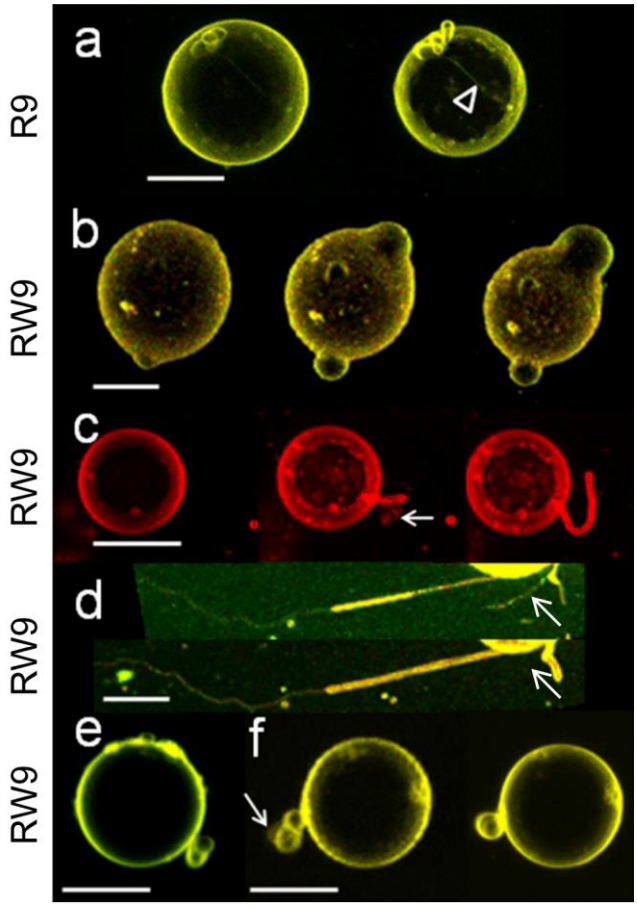

Fig. 2 Evolution of membrane protrusions of PMS after incubation with basic peptides. Confocal projections of PMS labelled with the fluorescent probe di-4-ANEPPDHQ. (**a**); PMS after incubation with R9 at 2 min. interval (left to right). Notice the internal tube (arrowhead) (see (Maniti et al., 2012)). (**b**); PMS at 20 and 50 min. intervals (left to right) after RW9 addition. (**c**); PMS at 20 min. intervals (left to right) after incubation with RW9. The "shadows" of the tube in the central image (arrow) are due to tube mobility. (**d**); Tubes from one PMS at 90 min. interval (top to bottom) after RW9 addition. Notice that the proximal part of the tube attached to the PMS is thicker than the distal part of the tube. The arrow indicate the retraction of a tube. (**e**); A rolling tube on a PMS surface after RW9 incubation. (**f**); PMS incubated with RW9 at 2 min. interval (left to right). Notice in (**e**) and at the left of (**f**) the shadows during the movement of a tube at the end of the rolling process (arrow). At right of (**f**) the rolled tube remains stable. Scale bars 10 μm.

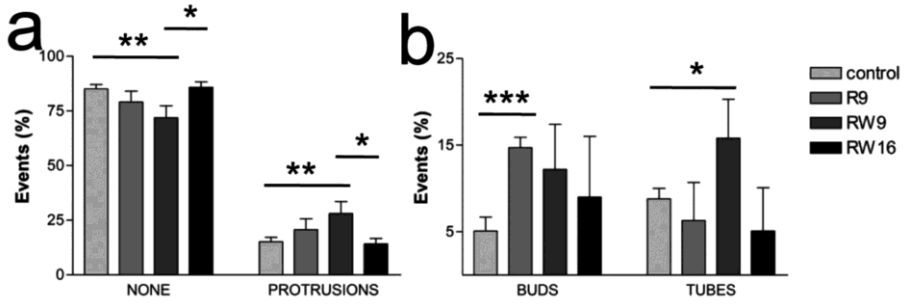

Fig. 3 Frequency of membrane protrusions induced by basic peptides. In (**a**), bars represent the percent of spherical PMS (none) and the percent of PMS with buds or tubes (protrusions). In (**b**), bars represent the percent of PMS with buds or with tubes in the whole PMS population. 3 855 PMS were analyzed. Bars are the mean +/- SEM from 2 to 4 independent experiments. * $P<0.05$, ** $P<0.01$, *** $P<0.001$

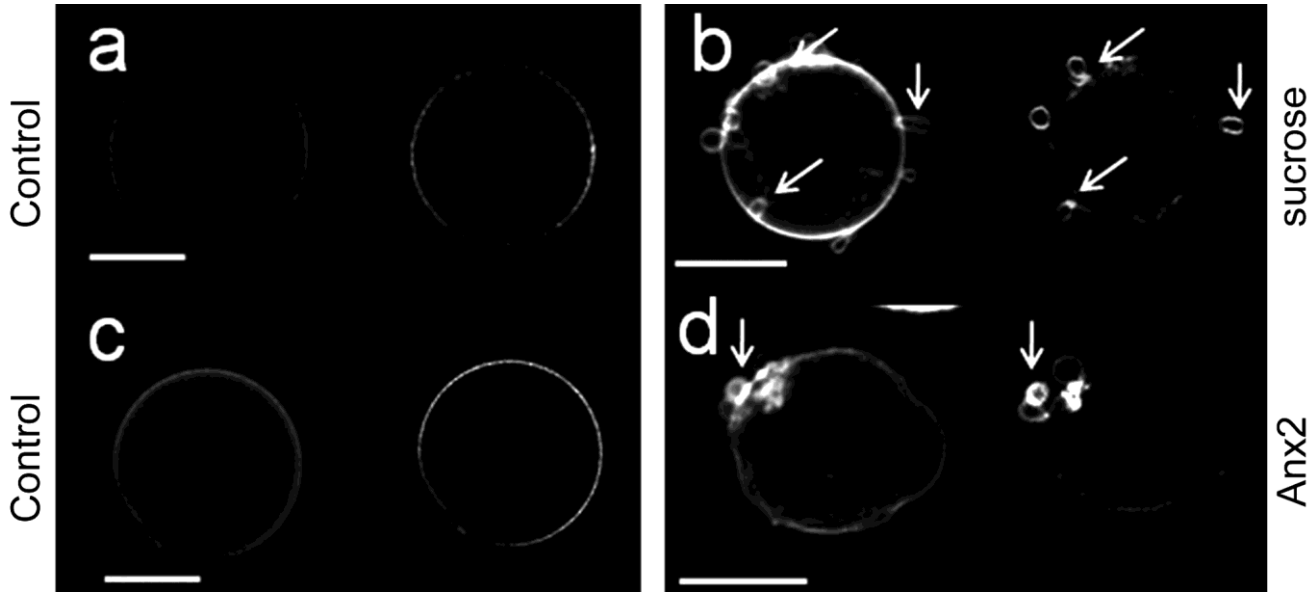

Fig. 4 RW9-induced membrane budding in hypertonic solution and in the absence of lipid fluorescent probe. (**a**); Confocal images of peptide-free PMS labelled with the fluorescent probe di-4-ANEPPDHQ 15 min. after sucrose addition. (**b**); PMS after RW9 incubation in 100 mM sucrose. (**c**); Confocal images of peptide-free PMS from Annexin 2-GFP transfected MDCK cells 90 min. after sample preparation under the microscope. Annexin 2-GFP is associated to the plasma membrane. (**d**); Annexin 2-GFP-PMS after RW9 incubation. At the left of the panels are the projections of 30 confocal slices, and at right a selected slice. Notice that the apparent internal vesicles are outward buds from the plasma membrane. Some buds are pointed by arrows. Scale bars 10 μm.

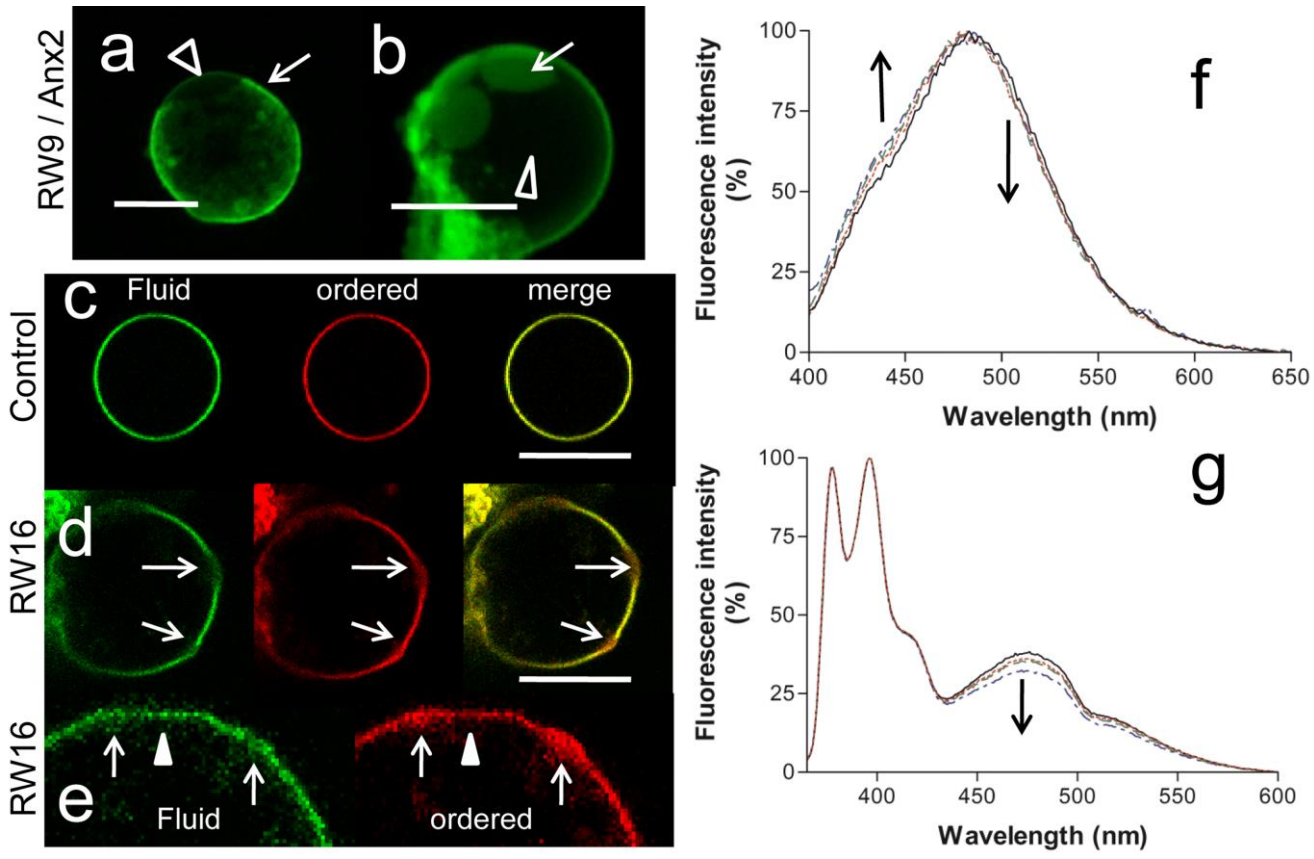

Fig. 5 Basic peptides provoke plasma membrane domain separation. Projections of 30 confocal slices from Anx 2-GFP-PMS incubated with RW9 (**a**,**b**). Notice the heterogeneous distribution of Anx 2-GFP compared with the control in Fig. 4c. Annexin 2-GFP rich domains (arrows), Anx 2-GFP poor domains (arrowheads). **c** and **d** are projections of three consecutive confocal slices of PMS labelled with the probe di-4-ANEPPDHQ (**c-d**). The colours code for the preferentially ordered rigid domains (570-590 nm in green) and the preferentially fluid domains (620-640 nm in red). Peptide-free PMS after 180 min. of labelling (**c**). PMS after RW16 addition (**d**). Zoom of a confocal slice (**e**) showing the differences in colour intensities (preferential fluid domains arrows, preferential rigid domain arrowhead). See Movies 4 and 5. Scale bars 10 μm. (**f**); Normalized Laurdan spectra of PC/PS LUVs (75/25) at 37°C. The increase of the rigid-ordered contribution (440 nm) and the decrease of the fluid domain contribution (490 nm) are indicated by arrows. (**g**); Normalized Py-met-chol spectra of PC/PS/PE/Py-met-chol LUVs (25/15/60/3) at 23°C. The decrease of probe dimers contribution (475 nm) is indicated by the arrow. LUVs (black lines), LUVs incubated with R9 (red dotted lines), RW9 (green dashed lines) and RW16 (blue dash-dotted lines).

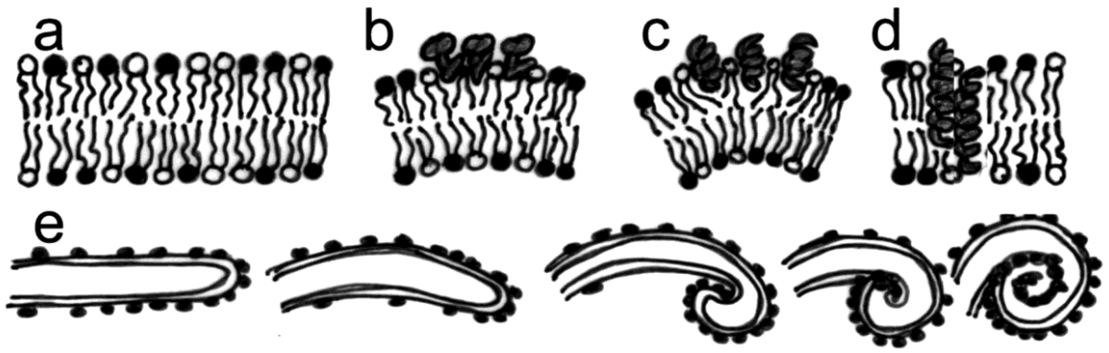

Fig. 6 Schematic model of membrane morphological changes induced by basic peptide-lipid interaction. (**a**); Membrane bilayer before peptide interaction. (**b**); R9 (gray structures) interacts with the phospholipid head groups by guanidine hydrogen bonding creating a small separation between them. (**c**); The amphipathic α-helix of RW9 (small gray helix) is able to snorkel into the external leaflet creating stronger separation of phospholipids and thus stronger positive curvature. (**d**); The amphipathic α-helix of RW16 (long gray helix) is able to insert profoundly into the bilayer inducing a small change in membrane curvature. To allow membrane insertion of the amphipathic helix molecules of RW16 will associate by the arginines thanks to ionic salt bridges. Lipid domains separation is a consequence of specific peptide-lipid affinities. (**e**); Peptide redistribution as the driving force for rolling. Progressive accumulation of peptide in one side of the tube would change the positive curvature redistribution resulting in tube rolling and in formation of membranous multilayer structures at the cell surface. For more details see discussion